

Numerical Calculation of Thermal Blooming of Pulsed, Focused Laser Beams

PETER B. ULRICH

*Analysis Staff
Optical Sciences Division*

December 30, 1971



NAVAL RESEARCH LABORATORY
Washington, D.C.

DOCUMENT CONTROL DATA - R & D

(Security classification of title, body of abstract and indexing annotation must be entered when the overall report is classified)

1. ORIGINATING ACTIVITY (Corporate author)		2a. REPORT SECURITY CLASSIFICATION	
Naval Research Laboratory Washington, D. C. 20390		Unclassified	
3. REPORT TITLE		2b. GROUP	
A NUMERICAL CALCULATION OF THERMAL BLOOMING OF PULSED, FOCUSED LASER BEAMS			
4. DESCRIPTIVE NOTES (Type of report and inclusive dates)			
This is an interim report on a continuing problem.			
5. AUTHOR(S) (First name, middle initial, last name)			
Peter B. Ulrich			
6. REPORT DATE		7a. TOTAL NO. OF PAGES	7b. NO. OF REFS
December 30, 1971		20	9
8a. CONTRACT OR GRANT NO.		9a. ORIGINATOR'S REPORT NUMBER(S)	
NRL Problem R05-31-304		NRL Report 7382	
b. PROJECT NO.		9b. OTHER REPORT NO(S) (Any other numbers that may be assigned this report)	
ORD 0832-129-173-1, Task U1754-2			
10. DISTRIBUTION STATEMENT			
			
11. SUPPLEMENTARY NOTES		12. SPONSORING MILITARY ACTIVITY	
Exempt from distribution to Defense Documentation Center in accordance with DOD Instruction 5100.38		Dept. of the Navy (Naval Ordnance Systems Command), Washington, D. C. 20360	
13. ABSTRACT			
<p>This report summarizes the development of a computer program which solves the problem of propagation of pulsed, focused laser beams in a gas. The code includes the effects of the absorbing medium by self-consistent inclusion of the detailed hydrodynamic processes. The report presents a description of the transformations of the relevant equations, a description and stability analysis of the algorithms used, a summary of the checks on accuracy and internal consistency both of the wave optics and the hydrodynamics, comparison with analytic theories, and presentation of an example of results for a typical case of interest.</p>			

14. KEY WORDS	LINK A		LINK B		LINK C	
	ROLE	WT	ROLE	WT	ROLE	WT
Pulsed laser beams Transient effects Propagation Atmosphere Light transmission Nonlinear optics Thermal blooming Thermal lens effect						

CONTENTS

Abstract	ii
Problem Status	ii
Authorization	ii
INTRODUCTION	1
WAVE OPTICS	1
HYDRODYNAMICS	3
COMPUTATIONAL DETAILS	4
ACCURACY CHECKS	6
TYPICAL RESULTS	7
CONCLUSION	8
ACKNOWLEDGEMENT	8
REFERENCES	9
APPENDIX A - Stability Analysis	12
APPENDIX B - Flow Chart of Main Program	15

ABSTRACT

This report summarizes the development of a computer program which solves the problem of propagation of pulsed, focused laser beams in a gas. The code includes the effect of the absorbing medium by self-consistent inclusion of the detailed hydrodynamic processes. The report presents a description of the transformations of the relevant equations, a description and stability analysis of the algorithms used, a summary of the checks on accuracy and internal consistency both of the wave optics and the hydrodynamics, comparison with analytic theories, and presentation of an example of results for a typical case of interest.

PROBLEM STATUS

This is an interim report on a continuing problem.

AUTHORIZATION

NRL Problem R05-31-304
Project ORD 0832-129-173-1, Task U1754-2

Manuscript submitted December 13, 1971.

A NUMERICAL CALCULATION OF THERMAL BLOOMING
OF PULSED, FOCUSED LASER BEAMS

Peter B. Ulrich
Optical Sciences Division

I. INTRODUCTION

A numerical calculation of the thermal blooming¹ of pulsed, focused laser beams is described in this Report. This theory is complete in that it self-consistently takes into detailed account the hydrodynamic processes in the absorbing gas. For simplicity, only the case of a Gaussian initial beam, with no wind and no turbulence is considered. More realistic situations are now under investigation and will be covered in future Reports.

Previous work on this problem² is based upon models which sacrifice self-consistency in order to make the solution achievable by analytic methods. The present study will allow an assessment of the validity of this earlier work to be made.

Self-consistent investigations of steady, time-independent propagation have been made by several groups.^{3,4,5} The steady state is achieved after transients have decayed and only if there is a steady wind relative to the beam to sweep out the heated air. The present work can be used to study the transient response of a CW beam after turn-on and before the steady state is reached.

II. WAVE OPTICS

The wave optics theory as discussed in reference (4), is used here. If the times considered are restricted to be less than the transit time of a sound wave across any part of the beam then wind can be ignored and, unlike the problem of reference (4), this problem has cylindrical symmetry and the equation for propagation of light of amplitude, ψ , becomes,

$$2ik \frac{\partial \psi}{\partial z} + \frac{1}{r} \frac{\partial \psi}{\partial r} + \frac{\partial^2 \psi}{\partial r^2} + k^2(n^2 - 1) \psi = 0, \quad (1)$$

where z is the range, r measures distance radially from the beam axis, k is the radian number (ω/c), and $n(r,z,t)$ is the index of refraction

($n = 1$ for a vacuum). In equation (1), a term $\frac{2ik}{c} \frac{\partial \psi}{\partial t}$ has been dropped. This is tantamount to assuming an infinite speed for light velocity and neglects retardation of the effects of the beam.

It is convenient (and in some cases, necessary) to transform (1). The transformations and the utility of each are given here⁶.

$$(A) \quad \bar{r} = r/a_0$$

This normalizes the transverse dimension to a characteristic size describing the extent of the initial intensity distribution. In all cases studied here, a_0 is the radial distance at which the intensity of the initial Gaussian-distributed beam is down by a factor of $1/e$, at $z = 0$.

$$(B) \quad \zeta = z/ka_0^2$$

This converts the range into a fraction of the far field distance for a collimated beam. For focused propagation the utility of the transformation is that it simplifies the equation.

$$(C) \quad \tilde{r} = \bar{r} / \sqrt{D(\zeta)} \text{ where } D(\zeta) = \zeta^2 + (1 - \zeta/\bar{f})^2$$

and $\bar{f} = f/ka_0^2$, f being the focal point.

This transformation has the effect of making the extent of real space under study proportional to the size of the vacuum beam. $r(0)\sqrt{D}$ is the trajectory of a light ray in a diffraction limited Gaussian beam.

$$(D) \quad z = \int_0^{\zeta} \frac{d\zeta'}{D(\zeta')}$$

This further converts the range so that for equal size steps in Z , the smallest steps in occur at the waist of the vacuum beam. This is desirable since most of the effects occur in this region of high intensity which, therefore, must be sampled with high frequency.

$$(E) \quad \Phi(\tilde{r}, Z) = \sqrt{D(Z)\pi a_0^2} \exp \left[-i \frac{\tilde{r}^2 D(Z)}{2\zeta(Z)} \left(1 - \frac{\zeta(Z)/\bar{f}}{D(Z)} \right) \right] \psi(\tilde{r}, Z)$$

This phase and scale transformation removes the rapid phase oscillations in the radial direction and offsets the intensity behavior of the vacuum solution so that just the effect of interest, the departure in propagation from the unperturbed beam, is studied in detail.

Under the operation of these five transformations, Eq. (1) becomes,

$$2i \frac{\partial \Phi}{\partial Z} + \frac{1}{\tilde{r}} \frac{\partial \Phi}{\partial \tilde{r}} - \frac{\tilde{r}^2}{\tilde{r}^2} \Phi + k_a^2 (n^2 - 1) D(Z) \Phi = 0. \quad (2)$$

The beam intensity is given by,

$$I(\tilde{r}, Z, t) = \frac{P e^{-\alpha k_a^2 \zeta(Z)}}{\pi a_0^2 D(Z)} |\Phi|^2 \quad (3)$$

where P is the beam power and α is the linear absorption coefficient.

For $n^2 = 1$ the vacuum solution to (2) for an initial Gaussian focused distribution is,

$$\Phi_v(\tilde{r}, Z) = \frac{(1 - \zeta(Z)/\bar{f}) - i\zeta(Z)}{\sqrt{D(Z)}} e^{-\tilde{r}^2/2}, \quad (4)$$

where,

$$\zeta(Z) = \frac{\tan [Z - \tan^{-1}(1/\bar{f})] + 1/\bar{f}}{1 + 1/\bar{f}^2} \quad (5)$$

III. HYDRODYNAMICS

The laser beam is the heat source which gives rise to perturbations of the hydrodynamic quantities. Since the Fresnel approximation is predicated upon very slow variation of the beam in range it follows that the changes in the gas variables will be slowly varying in z as well. Axial fluid flow which is induced in one direction is almost exactly cancelled by flow in the opposite direction. The simplification of dropping the z -dependence of the density, pressure and velocity of the gas leads to the following linearized set of hydrodynamic equations for the symmetric problem.

Conservation of mass,

$$\frac{\partial \rho}{\partial t} + \rho_0 \left(\frac{\partial v}{\partial r} + \frac{v}{r} \right) = 0 \quad (6)$$

Conservation of momentum

$$\frac{\partial v}{\partial t} + \frac{1}{\rho_0} \frac{\partial p}{\partial r} = 0 \quad (7)$$

Conservation of energy

$$\frac{\partial p}{\partial t} + \gamma \rho_0 \left(\frac{\partial v}{\partial r} + \frac{v}{r} \right) = (\gamma - 1) \alpha I(r, z, t) \quad (8)$$

where ρ, v, p are small departures from ambient values, $\rho_0, v_0 (=0), p_0$ and γ is the ratio of specific heats. The right hand side of (8) represents the energy absorbed per second per unit volume by the intervening gas, and (3) supplies the beam intensity, I .

An additional transformation is applied to this set.

$$(F) \quad \tau = t/a_0 \sqrt{D(Z)}$$

This transformation allows time to elapse at each range in proportion to the vacuum beam size at that range, $a_0 \sqrt{D(Z)}$. This is desirable since effects develop more rapidly for smaller beams, all else being constant, due to the larger intensity. In this way is adequate sampling in time assured.

With these changes the hydrodynamic set becomes,

$$\frac{\partial \rho}{\partial \tau} + \rho_0 \left(\frac{\partial v}{\partial \tilde{r}} + \frac{v}{\tilde{r}} \right) = 0, \quad (9)$$

$$\frac{\partial v}{\partial \tau} + \frac{1}{\rho_0} \frac{\partial p}{\partial \tilde{r}} = 0, \quad (10)$$

$$\frac{\partial p}{\partial \tau} + \gamma p_0 \left(\frac{\partial v}{\partial \tilde{r}} + \frac{v}{\tilde{r}} \right) = (\gamma - 1) \alpha \sqrt{D(Z)} I(\tilde{r}, z, t) \quad (11)$$

where the original symbols for the hydrodynamic quantities as functions of the transformed variables should cause no confusion.

The induced change in refractive index of the gas is related to the density change by the Lorenz-Lorentz law,

$$n^2 - 1 = 3N\rho \quad (12)$$

where N is the refractivity.

IV. COMPUTATIONAL DETAILS

Two alternatives have been considered for the integration of Eqs. (9) through (12) together with (2). They differ in the order in which the time and range integrations are accomplished.

The first integrates in range, updating the gas variables at each step, all at a fixed time. The process is then repeated through the new values of hydrodynamic variables. This process of alternating

beam propagation in range and evolution of the gas in time is repeated until times of interest have evolved. The beam is seen to pass through a series of static representations of the gas, each separated by a time Δt , chosen small compared with hydrodynamic times which are of the order of the local beam size divided by the speed of sound.

When the total time span of interest is less than the time for sound waves to travel between any two adjacent range points, then one can safely reverse the order of time and range integration; i.e., time is evolved to the final time of interest at each range point before propagating the beam to the new range point. This method⁹, was used in a preliminary study⁷ of the transient response of the atmosphere to collimated beams. This latter method which was chosen for this work as well, is used to advantage when the time to be studied requires less steps in time than the range to be studied requires in range steps. This can be seen by reference to Table I where the storage locations required for each method are enumerated.

The table assumes that central differencing in range and time is used. This explains the entries of the number 3.

TABLE I
 ENUMERATION OF STORAGE REQUIREMENTS
 FOR ALTERNATIVE COMPUTING METHODS

<u>Variable</u>	<u>Method I</u> (march in z, fixed t)			<u>Method II</u> (march in t, fixed z)		
	r	z	t	r	z	t
Re ϕ	n_r	3	0	n_r	3	n_t
Im ϕ	n_r	3	0	n_r	3	n_t
ρ	n_r	n_z	3	n_r	0	3
v	n_r	n_z	3	n_r	0	3
p	n_r	n_z	3	n_r	0	3
TOTALS	$(6 + 9n_z)n_r$			$(6n_t + 9)n_r$		

(n_r, n_z, n_t = number of samples in r,z,t respectively).

The two methods are seen to require comparable storage when $n_z \approx n_t$. This condition is met when studying pulses of a few hundred microseconds or greater at modest ranges or when the focusing is not too great. For times much longer than this the inclusion of wind becomes necessary. Wind introduces an asymmetry which effectively replaces n_r by $n_r^2/2$ in the above enumeration making storage requirements prohibitively large.

The stability of the central differencing of the wave optics equation was reported in reference (4). The symmetry of the present problem does not change those arguments. It was found for the hydrodynamic set that forward differencing in time was unstable as well, and that central differencing (two-point prediction) produced a stable algorithm. The stability of the hydrodynamics is discussed in Appendix A. Appendix B is a flowchart of the main program of the pulse code.

V. ACCURACY CHECKS

Computer solutions of (2) with $n^2 = 1$ were compared point by point with expression (4) for all ranges and radii. Agreement was always better than one part in 10^3 in amplitude, Φ_v . This was true even for cases of extremely large mirrors (1 meter diameter) and short focal lengths (tens of meters). This success is due to the transformations described in Section II. The initial surfaces of constant phase for a focused Gaussian beam are approximately spherical surfaces centered at the focal point. In the original coordinate system the values of the amplitude are specified on planes perpendicular to the z-axis and not on the surfaces of constant phase so that the amplitude goes through oscillations. The phase grows with the square of the radius of the mirror so that for large mirrors extremely fine sampling is required to faithfully sample the transverse oscillations. The transformation (E) removes this phase throughout the path so that the real and imaginary parts of the amplitude are Gaussian in radius, and hence easily sampled to produce the accuracy noted above. Any further phase changes will be induced by refraction through the thermal lens and this is expected to be an effect free from rapid oscillations in radius.

During the course of the computation the integrated intensity is checked for constancy,

$$\int_0^{\infty} |\Phi|^2 \tilde{r} d\tilde{r} = \text{constant}, \quad (13)$$

at each z-plane for all time. This condition is obeyed to better than 1 part in 10^3 and even this error can be largely attributed to edge effects; the integration is not over an infinite path but typically carried out to six e-folding distances in radius.

The hydrodynamic accuracy is checked at selected Z-planes for all times by separately monitoring the right and left hand side of the integral form of the continuity equation,

$$\frac{\partial}{\partial t} \int \rho dV = - \oint \rho \vec{v} \cdot d\vec{s} \quad (14)$$

where V is a volume element and $d\vec{s}$ an outwardly directed surface element. In the computer code the integration is taken over a cylinder of unit length in Z so that (14) becomes, in scaled variables,

$$\frac{\partial}{\partial \tau} \int_0^{\tilde{r}} \rho(\tilde{r}') \tilde{r}' d\tilde{r}' = - \tilde{r} \rho_o v(\tilde{r}) \quad (15)$$

The numerical integration is done by the trapezoidal rule. The relation is checked for each r-value sampled. Agreement is found to be better than 1/2% which is the limit of accuracy of the trapezoidal integration for the step size in radius used.

For very short times and at ranges near the laser face the density changes are essentially due to the vacuum beam. A perturbation theory² expression for ρ should apply,

$$\rho = (\gamma - 1) \alpha t^3 \nabla^2 |\Phi_v|^2 / 6 \quad (16)$$

where Φ_v is given by Eq. (4). Agreement with this expression is achieved for small enough step size, so that this expression is used as a very sensitive criterion for choosing accurate step sizes for the whole time evolution.

A wave optics perturbation calculation⁸ predicts that the ratio of on-axis intensity at the end of the pulse of length t at the focal point to the vacuum intensity there is given by,

$$\frac{|\Phi|^2}{|\Phi_v|^2} = 1 - \left(\frac{1}{16} \text{Log } 9 + \frac{1}{6} \right) \frac{3N}{2} \frac{(\gamma - 1) \alpha t^2 E}{\pi} \frac{k^4 a_o^2}{f^2} \quad (17)$$

where $E = Pt$, the total energy delivered. This behavior is confirmed qualitatively only for beams which are not strongly focused since the perturbation theory assumes refraction due to the undistorted beam.

VI TYPICAL RESULTS

The program, at its present stage of development, provides plots of the beam intensity vs. radius normalized to the vacuum intensity

($\tau = 0$), for selected times at selected ranges. Figures 1 and 2 show typical output for a beam focused at 3 kilometers with an initial half-meter diameter ($a_0 = 17.68$ cm) and a power sufficient to supply 700 joules in 70 microseconds.

The ranges shown are $z = 2.584$ km in Fig. 1 and $z = 3.0$ km, the focal point, in Fig. 2. Note the enhanced intensity off-axis at 70 microseconds at the 2.584 km range. The beam is not strongly focused at this range and this behavior is in qualitative agreement with collimated beam predictions^{2,7}. The intensity maximum at this point causes local heating with a concomitant drop in density. The light rays passing through this region will be refracted both away from and into the center of the beam to produce the smooth wide distribution at the focal point as is seen in Fig. 2 at about the same time.

Fig. 3 is a plot of intensity vs radius for the same beam as portrayed in Figs. 1 and 2 except the curves are for different ranges at the same 70 microsecond time. The development of the off-axis intensity at 2.5 km and the subsequent broadening of this peak is clearly evident.

VII. CONCLUSION

This report has summarized the development of a computer program for studying the self-consistent time dependent propagation of focused laser beams in gases leading to thermal blooming. This work represents a significant extension of earlier analytic work and establishes the foundation for a realistic study of propagation effects in situations of practical interest.

VIII. ACKNOWLEDGEMENT

The author gratefully cites the encouragement of Dr. John N. Hayes with whom he has had numerous useful conversations concerning this problem.

REFERENCES

1. When a laser beam passes through a gas, energy that is extracted from the beam eventually appears as a perturbation in the ambient density of the gas. If the product of beam intensity times the absorption coefficient of the gas is sufficiently large, the resultant density changes represent index of refraction changes sufficient to measurably alter the propagation of the beam. This effect is known as "thermal blooming" or "the thermal lens effect."
2. Hayes, J. N., NRL Report 7213, Feb 11, 1971; also to be published in *Applied Optics*, 11 March (1972) Analogous work has been reported by Kenemuth, J. R., Hogge, C. B., Butts, R. R., and Avizonis, P. V. in *Laser Division Digest*, Air Force Weapons Laboratory, Kirtland AFB, N.M. Dec 1971, p. 74 and by Butts, R. R., same report, p. 95.
3. Wallace and Camac, *J. Opt Soc.* 60, 1587, (1970).
4. Aitken, A. H., Hayes, J. N., and Ulrich, P. B., *J. Opt. Soc. Am.* 61, 674, (1971). Also in NRL Report 7293, May 28, 1971, and to be published *Applied Optics*, 10, Feb (1972).
5. Herrmann, J. and Bradley, L. C., Report LTP-10, Lincoln Laboratory, Lexington, Massachusetts.
6. Analogous transformations are used in the CW computer studies (cf. references (2), (3), and (4)) but their usefulness is much reduced due to lack of circular symmetry in the transverse plane.
7. Ulrich, P. B. and Wallace, J., to appear.
8. Ulrich, P. B., NRL Report, in preparation.
9. The possibility of doing the time integration for all time at a fixed range was suggested to the author by J. Wallace, Jr. of AVCO-Everett.

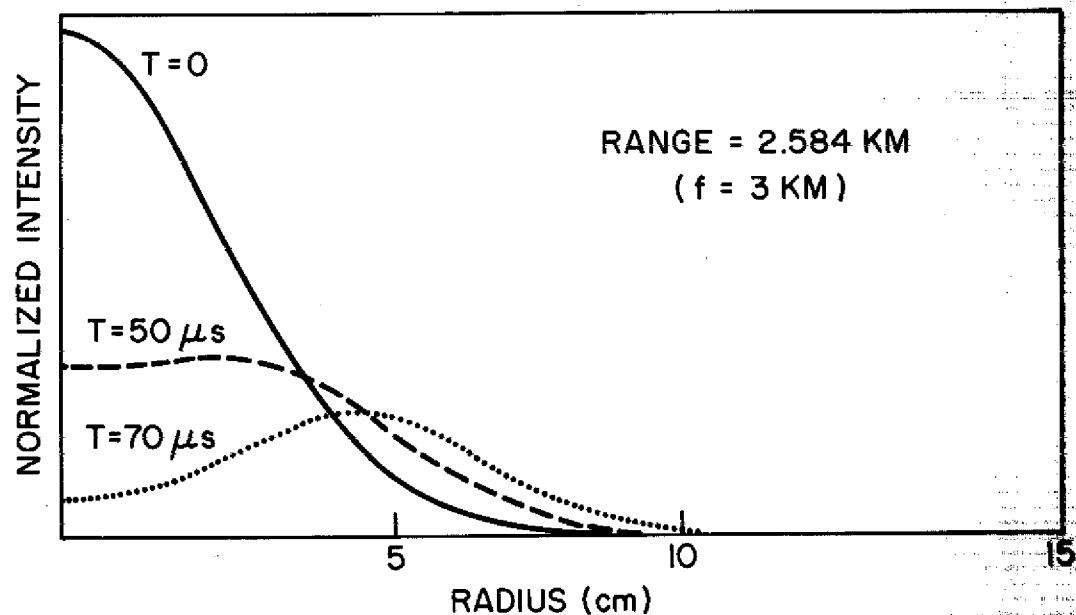


Fig. 1. Plot of normalized intensity vs radius for a half-meter optics laser beam focused at three kilometers, for three times after arrival of leading edge of pulse at $z = 2.584$ km.

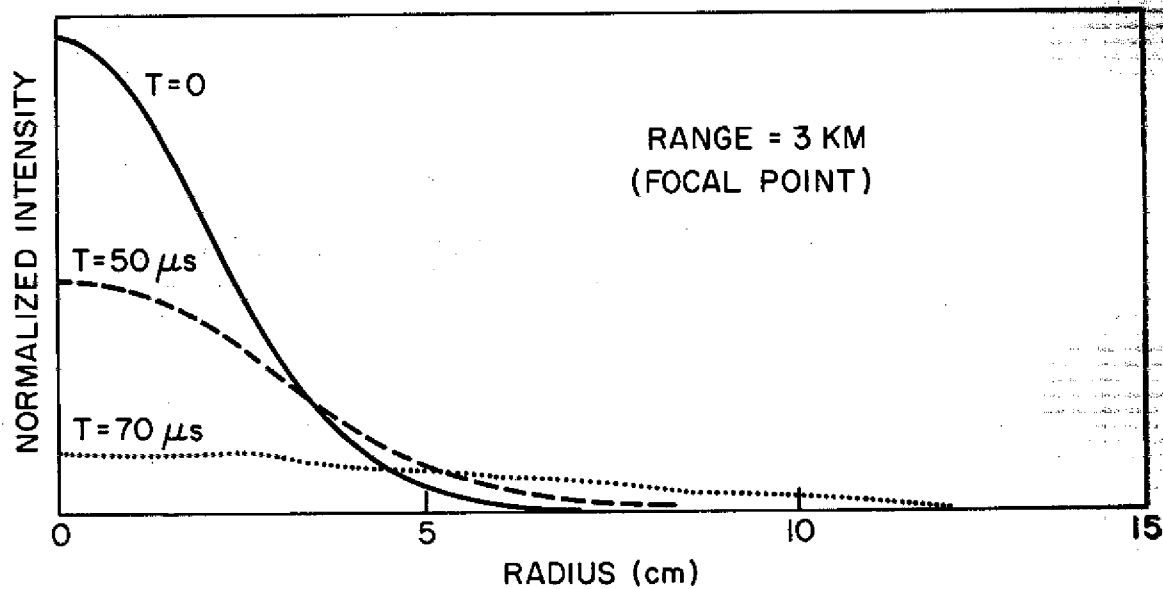


Fig. 2. Same beam as shown in Fig. 1 but at $z = 3.0$ km, the focal point.

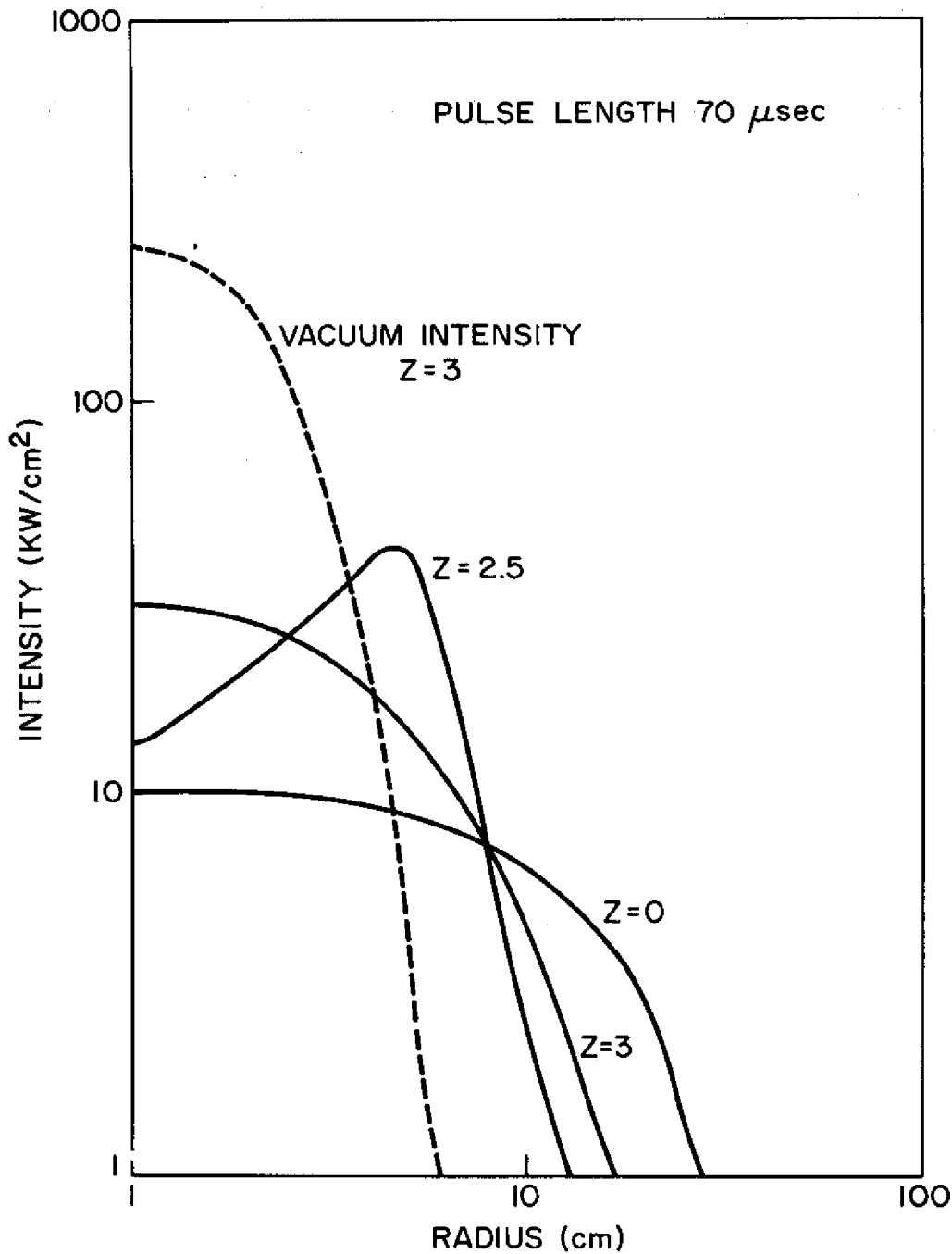


Fig. 3. Log-Log plot of absolute intensity in KW/cm² vs radius for three ranges, $z = 0$, $z = 2.5$ km and $z = 3.0$ km, all at 70 microseconds after arrival of pulse at each range. Also shown is the vacuum profile at the focal point, 3.0 km. This all for the same beam as appears in Figs. 1 and 2.

Appendix A

STABILITY ANALYSIS

The numerical stability of Eq. (2) is covered by the analysis of reference (3). The stability of the set (9) through (11) is discussed here. Round-off errors are propagated by the same equations with the right hand side of (11) set equal to zero. Using central differences throughout gives for the error terms, ρ_e , v_e , and p_e ,

$$\frac{\rho_e(\tilde{r}, t+\Delta t) - \rho_e(\tilde{r}, t-\Delta t)}{2\Delta t} = -\rho_0 \left[\frac{v_e(\tilde{r}+\Delta\tilde{r}, t) - v_e(\tilde{r}-\Delta\tilde{r}, t)}{2\Delta\tilde{r}} + \frac{v_e(\tilde{r}, t)}{\tilde{r}} \right] \quad (\text{A-1})$$

$$\frac{v_e(\tilde{r}, t+\Delta t) - v_e(\tilde{r}, t-\Delta t)}{2\Delta t} = -\frac{1}{\rho_0} \left[\frac{p_e(\tilde{r}+\Delta\tilde{r}, t) - p_e(\tilde{r}-\Delta\tilde{r}, t)}{2\Delta\tilde{r}} \right] \quad (\text{A-2})$$

$$\frac{p_e(\tilde{r}, t+\Delta t) - p_e(\tilde{r}, t-\Delta t)}{2\Delta t} = -\gamma\rho_0 \left[\frac{v_e(\tilde{r}+\Delta\tilde{r}, t) - v_e(\tilde{r}-\Delta\tilde{r}, t)}{2\Delta\tilde{r}} + \frac{v_e(\tilde{r}, t)}{\tilde{r}} \right] \quad (\text{A-3})$$

A Fourier-Bessel decomposition of the dependent variables is made,

$$\rho_e(\tilde{r}, t) = \int_0^{\infty} kdkR(k, t) J_0(k, \tilde{r}) \quad (\text{A-4})$$

$$v_e(\tilde{r}, t) = \int_0^{\infty} kdkV(k, t) J_1(k, \tilde{r}) \quad (\text{A-5})$$

$$p_e(\tilde{r}, t) = \int_0^{\infty} kdkP(k, t) J_0(k, \tilde{r}) \quad (\text{A-6})$$

where $J_1(k\tilde{r})$ is used in (A-5) since $v(0, \tau)$ is set equal to zero for all τ so that $v_e(0, \tau)$ is identically zero; i.e., there is no error in $v(\tilde{r}, t)$ at the origin. (No confusion should arise here with the use of k as a transverse mode number and the wave number of the optical beam in the main text).

Substituting the above decompositions into the algorithm (A-1, 2, 3) and Taylor expanding the Bessel functions to order $(\Delta\tilde{r})^3$ gives,

$$\frac{R(k, t+\Delta t) - R(k, t-\Delta t)}{2\Delta t} = -\rho_0 V(k, t) \quad (\text{A-7})$$

$$\frac{V(k, t+\Delta t) - V(k, t-\Delta t)}{2\Delta t} = + \frac{k}{\rho_0} P(k, t) \quad (\text{A-8})$$

$$\frac{P(k, t+\Delta t) - P(k, t-\Delta t)}{2\Delta t} = -\gamma \rho_0 k V(k, t) \quad (\text{A-9})$$

A Fourier decomposition in time is made and the Imaginary part of the frequency is studied to determine potential exponential growth or decay of each mode associated with the transverse wave number, k .

Thus, let,

$$R(k, t) = \alpha(k) e^{i\omega t} \quad (\text{A-10})$$

$$V(k, t) = \beta(k) e^{i\omega t} \quad (\text{A-11})$$

$$P(k, t) = \delta(k) e^{i\omega t} \quad (\text{A-12})$$

These quantities are substituted into (A-7,8,9) to get a set of homogeneous linear equations for α , β , and δ . A necessary and sufficient condition for a solution is the vanishing of the determinant of the coefficients,

$$\begin{vmatrix} 2i\sin\omega\Delta t & 2\rho_0 k\Delta t & 0 \\ 0 & 2i\sin\omega\Delta t & \frac{-2k}{\rho_0} \Delta t \\ 0 & 2\gamma\rho_0 k\Delta t & 2i\sin\omega\Delta t \end{vmatrix} = 0 \quad (\text{A-13})$$

One solution is $\omega = 0$ which is always stable. The other two modes satisfy

$$\sin^2 \omega\Delta t = c_s^2 k^2 \Delta t^2 \quad (\text{A-14})$$

where, $c_s^2 \equiv \gamma\rho_0/\rho_0$.

Now let $\omega = \xi + i\eta$ so that $\text{Im}\omega = \eta > 0$ predicts damping of errors, $\exp(-\eta t)$. Equating real and imaginary parts gives the dispersion relation,

$$\eta = \frac{1}{\Delta t} \cosh^{-1}(c_s k \Delta t)$$

(A-15)

Now η is zero until $c_s k \Delta t > 1$; at that point

$$\left. \frac{\partial \eta}{\partial k} \right|_{k = \frac{1 + \epsilon}{c_s \Delta t}} = \frac{1}{\sqrt{(1 + \epsilon)^2 - 1}} c_s > 0$$

(A-16)

so the positive branch of (A-15) is chosen and $\eta > 0$, predicting damping of errors and a stable algorithm.

By way of contrast the use of forward differencing in time leads to the following dispersion relation,

$$i\xi \Delta t - \eta \Delta t = \ln \left(\sqrt{1 + c_s^2 k^2 \Delta t^2} \right) \pm i \tan^{-1}(c_s k \Delta t)$$

(A-17)

Equating of real and imaginary parts gives $\text{Im} \omega = \eta < 0$, and thus, growth of errors. Forward differencing is unstable.

APPENDIX B
 FLOW CHART OF MAIN PROGRAM

